HHS Public Access

Author manuscript

Anal Chem. Author manuscript; available in PMC 2020 January 07.

Published in final edited form as:

Anal Chem. 1987 January 15; 59(2): 271–278. doi:10.1021/ac00129a012.

Resolution of Multicomponent Fluorescence Emission by Phase Sensitive Detection at Multiple Modulation Frequencies

Susan M. Keating-Nakamoto, **Henryk Cherek**[1], **Joseph R. Lakowicz**

School of Medicine, University of Maryland at Baltimore, 660 West Redwood Street, Baltimore, Maryland 21201

Abstract

Phase sensitive emission spectra recorded at multiple frequencies were used to determine the lifetimes and steady-state spectra of the fluorophores In two-component mixtures. This analysis does not require any previous knowledge of the lifetimes, fractional Intensities, or the emission spectra and is thus an Improvement over single frequency phase sensitive detection which requires known emission spectra or known lifetimes. Phase sensitive emission spectra are recorded at several frequencies and arbitrarily chosen detector phase angles. The data are analyzed by use of nonlinear least squares to recover the lifetimes and wavelength-dependent fractional Intensities. The latter values determine the emission spectrum and relative intensity of each component in the mixture. Using this technique, we resolved two-component mixtures of fluorescein and 9-amlnoacrldlne, 2-(*p*-toluidinyl)-naphthalene-6-sulfonlc acid and 6-proplonyl-2-(dlmethylamlno)naphthalene, and *N*-acetyl-L-tyrosinamide and *N*-acetyl-L-tryptophanamide. In these mixtures the lifetimes differ by about 2-fold. Analysis of simulated data is presented to Illustrate the requirements for a satisfactory resolution. For simulated two-component mixtures, the components can be resolved If the lifetimes differ by 2-fold or greater, even with extensive overlap of the emission spectra.

Registry No.

Fluorescein, 2321-07-5; 9-aminoacridine, 90-45-9; 2-(*p*-toluidinyl)naphthalene-6-sulfonic acid, 7724-15-4; 6-propionyl-2-(dimethylamino)naphthalene, 70504-01-7; *N*-acetyl-L-tyrosinamide, 1948-71-6; *N*-acetyl-L-tryptophanamide, 2382-79-8

Fluorescence spectroscopy and the measurement of fluorescence decays is frequently used in the chemical, physical, and biological sciences. For example, fluorescence decays have been widely used to determine the behavior of fluorophores that are bound to macromolecules (1–5). The fluorescence decays are usually complex, due to the presence of more then one fluorophore or to the intrinsically complex decays of even single fluorophores. Regardless of whether the fluorescence is being used for analytical purposes, such as determining the amount of bound species in an immunoassay, or as a probe of a macromolecule, it is often necessary to determine the parameters that describe the heterogeneous emission, these being the lifetimes and fractional intensities in the decay law.

[1]On leave from Nicholas-Copernicus University, Torun, Poland.

Both the time-domain (4–7) and phase-modulation (7–13) techniques for the measurement of these decays have improved significantly in recent years. In particular, the recent appearance of variable frequency phase fluorometers (14, 15) permit measurements up to 2 GHz (16) and allow resolution of complex lifetimes and anisotropy decays even on the picosecond time scale (17). Furthermore, the time resolution of time-correlated single photon counting has been increased by the introduction of picosecond dye laser sources (18–20).

Until recently, commercially available phase fluorometers permitted measurement at only two or three modulation frequencies. Due to the limited frequencies and lack of stability these instruments were not generally useful for the resolution of mixtures. Two-component mixtures could be resolved (8–11, 21, 22), but the solutions were generally unreliable. A modification of the phase-modulation method, phase sensitive detection (PSD), was also used to study multicomponent decays to enhance the resolution of the single frequency measurements (23, 24). This technique, which relies on a difference in the lifetimes of the components, has been used to resolve multicomponent fluorescence decays (23–30) to separate Raman, phosphorescence, and fluorescence components (31, 32) and to study excited-state reactions which shift the emission spectra (33, 34). We recently reported (35, 36) a new approach to the measurement and analysis of phase sensitive (PS) data which led to the resolution of three-component mixtures by using data measured at only one frequency. This method appears to be the only one that permits resolution of three decay times using data from only one frequency. Yet the procedure is limited in that it requires measurement or knowledge of the normalized spectral distribution of each component. This is a serious restriction, which is impossible to satisfy in many situations, especially those involving macromolecules. To eliminate this restriction, we used the increased information content by measuring phase sensitive emission spectra at multiple modulation frequencies.

In this new procedure, phase sensitive emission spectra are collected at several detector phase angles per frequency over a wide frequency range. The data are then analyzed by using nonlinear least squares, to recover the lifetimes and the fractional intensity of each component at each wavelength. The fractional intensities determine the individual emission spectra of each component in the mixture. Although this method yields the correct emission spectra and lifetimes, some problems remain to be solved. These include the long times required for data acquisition due to the large amount of data required for good resolution of the mixtures. An inadequate amount of data can result in a lack of precision in the recovered parameters. However, this method of multicomponent analysis may be valuable in the analysis of complex systems of chromophores, such as the photosynthetic pigments, in which the emissions are dispersed over a range of wavelengths (37). Our use of PSD is different from that of McGown and Bright (27–29) or Gratton and Jameson (30). McGown and Bright independently measure the phase sensitive intensities of each component and fit the phase sensitive intensities of the mixture which are measured at only one or two frequencies. The latter group uses known lifetime values to calculate the fractional intensities and record the phase resolved spectra of each component. Our method is more general in that neither the lifetimes nor the emission spectra are required for the analysis.

THEORY

Theory of Phase Sensitive Fluorescence.

The theory of phase modulation spectroscopy has been extensively described (1, 7, 12, 38) and will only be briefly discussed here. In phase fluorometry a sample is excited with intensity-modulated light. The fluorescence emission is modulated and is a forced response to the excitation. The emission is delayed by a phase angle (θ) and demodulated (m) relative to the exciting light

$$F(t) = 1 + m \sin(\omega t - \theta) \tag{1}$$

In this expression $\omega = 2\pi F$ is the circular modulation frequency where F is the frequency in hertz. For a single-component solution with a single exponential decay, the lifetime (τ) is related to m and θ by

$$\tan\theta = \omega\tau \tag{2}$$

$$m = \left(1 + \omega^2\tau^2\right)^{-1/2} \tag{3}$$

The values of m and θ are determined by the fluorescence lifetime and frequency of the exciting light. For multicomponent samples the emission is a weighted sum of the constant and modulated intensities of each component i. The measured values of m and θ for the mixture and eq 2 and 3 yield only apparent lifetimes. The values of m_i and θ_i for each component, or equivalently the lifetimes, must be determined by a more complex procedure (12).

In PSD the emission spectrum is scanned as usual but the phase-sensitive detector (lock-in amplifier) detects only the modulated portion of the emission. The PS detector yields an unmodulated signal, I_p, that is a weighted sum of the modulated emission of each component

$$I_p(\lambda, \theta_D, \omega) = kI_{ss}(\lambda)\sum_i f_i(\lambda)m_i \cos\left(\theta_D - \theta_i\right) \tag{4}$$

Here, λ is the emission wavelength, θ_D is the detector phase angle relative to the incident light, k is a constant, $I_{ss}(\lambda)$ is the steady-state spectrum of the mixture, and $f_i(\lambda)$ is the wavelength-dependent fractional intensity of the ith component. The spectrum of each component in the mixture is given by

$$I_i(\lambda) = f_i(\lambda)I_{ss}(\lambda) \tag{5}$$

At any frequency and θ_D, the PS intensity of each component is proportional to both its fractional intensity and the cosine of the phase difference between its emission and the detector phase angle, cos ($\theta_D - \theta_i$). Therefore, for each component, as θ_D is varied, the value of cos ($\theta_D - \theta_i$) will change, altering the phase sensitive intensity and the spectral

shape. This dependence of the PS spectra on θ_D is the basis for calculating the individual lifetimes and fractional intensities from the spectra.

If PS spectra are measured at one modulation frequency, the information is limited. First, the lifetimes of the fluorophores must be appropriate for the available frequency. A more severe limitation is that the emission spectra cannot be calculated unless the lifetimes are known (30), and the lifetimes cannot be calculated unless the spectra are known (24, 25). For example, in their resolution of the individual spectra Gratton and Jameson (30) were required to use the independently measured lifetimes of each component. In our previous method (24, 25) the lifetime of each component is found by suppressing the emission of one component and matching the phase sensitive spectrum with a known emission spectrum. These restrictions can be avoided if the data are collected at multiple modulation frequencies. At each wavelength the frequency-dependent phase sensitive intensities define the frequency-dependent phase angles. In essence, this defines the decay law at each wavelength. Since the data are obtained across the emission spectra, the data determine both the emission spectra and the lifetimes of the components. A second advantage of a variable frequency instrument is the ability to select modulation frequencies that are best suited for resolution of the decay times of the sample. In contrast, data at one modulation frequency determine only the phase angle at this frequency, which is not adequate to determine the lifetimes and spectra of two components.

Measurements and Data Analysis.

We simultaneously measure three spectra. Two phase sensitive spectra are measured: an in-phase spectrum (I_p) at detector phase θ_D, and a quadrature spectrum (I_Q) at $\theta_D + 90°$. We also measure the total amplitude (vector sum) of the in-phase and quadrature signals of the modulated emission (I_m), at the same gain as the PS spectra. I_m is available as a direct output of the lock-in amplifier. The magnitude spectrum is proportional to the steady-state spectrum after attenuation of each component by m_i

$$I_m(\lambda,\omega) = kI_{ss}(\lambda)\sum_i f_i(\lambda)m_i \tag{6}$$

In the analysis, the measured $I_p(\lambda,\theta_D,\omega)$ and $I_q(\lambda,\theta_D + 90°,\omega)$ spectra are divided by $I_m(\lambda,\omega)$ to form PS ratio spectra, R_p and R_q, as described by

$$R_p = \frac{I_p(\lambda,\phi_D,\omega)}{I_m(\lambda,\omega)} = \frac{\sum_i f_i(\lambda)m_i\cos\left(\phi_D - \phi_i\right)}{\sum_i f_i(\lambda)m_i} \tag{7}$$

and

$$R_q = \frac{I_q(\lambda,\phi_D + 90°,\omega)}{I_m(\lambda,\omega)} = \frac{\sum_i f_i(\lambda)m_i\cos\left(\phi_D + 90° - \phi_i\right)}{\sum_i f_i(\lambda)m_i} \tag{8}$$

This normalization corrects for drifts in light intensity or the extent of modulation during data collection, and the PS intensities are scaled from −1 to +1. However, this division

eliminates any information that may have been available from the frequency-dependent amplitude of the modulated emission. The use of the amplitude information would require that all the phase sensitive spectra be collected at the same gain and with the same degree of modulation of the incident light. These are difficult experiment constraints, which we have not implemented. The ratio spectra are fit in an iterative manner to calculated spectra using assumed values for the lifetimes, τ_{ci}, and fractional intensities of each component at each wavelength, $f_{ci}(\lambda)$. The subscript c is used to indicate the calculated or assumed values of τ_i and $f_i(\lambda)$. The values of $f_{ci}(\lambda)$ and τ_{ci}, are varied to obtain the best match between the measured (R_p and R_q) and calculated (R_{cp} and R_{cq}) ratio spectra. We use the procedure of nonlinear least squares, based on the Marquardt algorithm as described by Bevington (39). The analysis is a modification of that previously reported for analysis of single frequency PS data (35, 36). It should be noted that the analysis assumes the decay times are constant for each component across the emission spectrum. Hence, our analysis might be regarded as a global method, as defined by Brand and co-workers (6).

The goodness-of-fit is determined by searching for the minimum value of χ_R^2, which is the error-weighted sum of the squared deviations between the measured and calculated data

$$\chi^2 = \sum_{\lambda}\sum_{\theta_D}\sum_{\omega} 1/\sigma^2\left[R_p(\lambda,\theta_D,\omega) - R_{cp}(\lambda,\theta_D,\omega)\right]^2 + 1/\sigma^2\left[R_q(\lambda,\theta_D+90°,\omega) - R_{cq}(\lambda,\theta_D+90°,\omega)\right]^2 \quad (9)$$

The weighting factor (σ) is

$$\sigma = 0.01S \quad (10)$$

where S is the estimated percent noise in the data. The final values of τ_{ci} and $f_{ci}(\lambda)$ are those which minimize χ^2. The goodness of fit is judged by the value of the reduced χ^2

$$\chi_R^2 = \chi^2/\nu \quad (11)$$

where ν is the number of degrees of freedom

$$\nu = N_\lambda N_D N_\omega - p \quad (12)$$

N_λ is the number of emission wavelengths, N_D the number of detector phase angles, N_ω the number of frequencies, and p the number of floating parameters (one for each component τ_{ci} and one for each $f_{ci}(\lambda)$ after the first component). For values of τ_{ci} and $f_{ci}(\lambda)$ which adequately describe the data the value of χ_R^2 is expected to fluctuate near 1.0, assuming the data contain only random experimental errors. The values of $f_{ci}(\lambda)$ are used to calculate the emission spectrum of each component, $I_i(\lambda)$, using eq 5.

A discussion of the weighting factor and the detailed equations for the analysis are given in the Appendix.

EXPERIMENTAL SECTION

Materials.

9-Aminoacridine (9-AA), *N*-acetyl-L-tyrosinamide (NATyrA), *N*-acetyl-1-tryptophanamide (NATA), and *p*-terphenyl (p-ter) were obtained from Aldrich Chemical Co., Inc., 6-propionyl-2-(dimethylamino)naphthalene (PRODAN) and 2-(*p*-toluidinyl)naphthalene-6-sulfonic acid (TNS) were from Molecular Probes, Inc., *p*-bis[2-(5-phenyloxazolyl)]benzene (POPOP) was from Eastman Laboratory and Speciality Chemicals, and Ludox was from E. I. du Pont de Nemours Co., Inc. These compounds were used without further purification, but fluorescein (FLS) was recrystallized. All chemicals, except Ludox, NATyrA, and NATA, were dissolved in 100% ethanol; Ludox was diluted into distilled water and NATyrA and NATA were diluted in 25 mM Tris–HCl, pH 7.5. All solutions were maintained at 20 °C. The samples were equilibrated with the atmosphere and were not purged with inert gas to remove dissolved O_2. The optical densities were below 0.16 at the excitation wavelengths.

Measurements.

The data were obtained with a continuously variable frequency phase fluorometer (15) and a lock-in analyzer (Model 5204 from EG & G, Princeton Applied Research). This instrument uses cross-correlation detection, which is accomplished within the photomultiplier tube (PMT). More specifically, the gain of the PMT is modulated by a small rf signal on its second dynode. This rf signal is at $F + 25$ Hz, where F is the modulation frequency of the incident light. The 25-Hz beat frequency contains the necessary phase and modulation information. Because of a sharp notch filter at 25 Hz, the data are not affected by nonsinusoidal modulation of the incident light or the PMT gain. The input signal to the lock-in analyzer was the modulated low-frequency (ac) signal from the sample. Previously, we electronically divided this signal by the root mean square value of a reference signal (35, 36). However, this did not seem necessary with the variable frequency instrument because of its greater stability. The present analysis of ratio spectra also cancels instrumental drift.

The laser excitation source for the PRODAN/TNS and FLS/9-AA mixtures was the He–Cd 325- and 442-nm lines, respectively. Data were collected at eight or nine frequencies from 2 to 108 MHz. For excitation of the NATyrA/NATA mixture, the light source was a 3.79162 MHz train of 5-ps pulses from a cavity dumped Coherent Model 700 dye laser containing rhodamine 6G as the dye. A second jet with the saturable absorber DODCI was present. The dye laser was synchronously pumped using a mode-locked Coherent Inova 15 argon-ion laser. The visible output of the dye laser was frequency doubled to obtain 285 nm using a Spectra Physics Model 390 frequency doubler with a KDP angle-tuned crystal. The UV excitation was attenuated 20-fold by using a neutral density filter to minimize photodecomposition of the sample. In this case the frequency synthesizer for the cross-correlation signal was phase locked to the cavity dumper. Seven modulation frequencies were used from 11.37486 to 113.7486 MHz. This instrument is the subject of a recent publication (16).

For all measurements, an emission polarizer was not used and the excitation polarizer was at 35° (40), except for the FLS/9-AA measurements at 0°. The emission band-pass was usually 8 nm, 16 nm for the PRODAN/TNS mixture, and data were collected at 5-nm steps.

The values of θ_D were relative to the following reference solutions: Ludox at 442 nm for the FLS/9-AA mixture, POPOP at 400 nm for the PRODAN/TNS mixture, and p-ter at 340 nm for the NATyrA/ATA mixture (24, 36). The lifetimes for the three reference solutions were taken as 0, 1.35, and 1.05 ns, respectively (41).

Steady-state spectra and lifetimes were measured under the same conditions and with the same instrument (15, 16). The individual lifetimes were measured so the recovered lifetimes could be compared with the expected values. The lifetimes were measured vs. Ludox, with the emission monochromator removed and a Corning 0–52 (PRODAN/TNS) or 3–72 (9-AA/FLS) cutoff filter in the emission path. For lifetime measurements both the phase and modulation values were measured and analyzed as previously reported (15, 41).

Data Analysis.

One objective of the analysis is to determine the correct number of components in the sample. Hence, a data set is typically fit several times, altering the number of assumed components. The values of χ_R^2 from the various fits are compared. If the value of χ_R^2 decreases significantly with the addition of another component to the decay law, the fit with the lower χ_R^2 is thought to best describe the data.

The VFPS data were fit to one-, two-, or three-component decays. In all cases the lifetimes and spectral distributions were floating parameters, but the program permits any of the parameters to be held constant. In the analysis, the values of $f_{ci}(\lambda)$ float relative to those of the first component. The $\sum_i f_{ci}(\lambda)$ is then normalized to 1.0 at each wavelength. For example, for a two-component fit over 20 wavelengths, there are 22 floating parameters. Therefore, the number of degrees of freedom for a typical data set containing PS data recorded at 12 θ_D (6 I_p and 6 I_q) and 7 frequencies will be 1658. According to Bevington (39) a difference in χ_R^2 for two fits of 1.3 would be statistically large enough to reject the fit with the larger value of χ_R^2 with less than a 1% probability of error. However, we generally accept the more complex fit only if it yields a 2-fold decrease in the relative values of χ_R^2.

Simulated Data.

PS data were simulated as R_p and R_q using eq 7 and 8. The values of $f_i(\lambda)$ were calculated as

$$f_i(\lambda) = \frac{g_i I_i^n(\lambda)}{I_{ss}(\lambda)} \tag{13}$$

For the ith component g_i is the steady-state fractional intensity, $\sum_i g_i = 1.0$, and $I_i^n(\lambda)$ is its area normalized emission spectrum. $\sum_\lambda I_i^n(\lambda) = 1.0$. The steady spectrum of the mixture is described using

$$I_{ss}(\lambda) = \sum_i g_i I_i^n(\lambda) \quad (14)$$

The $I_i^n(\lambda)$ spectra were simulated by use of Gaussian distributions. In all cases $g_1 = g_2 = 0.50$, with 50 nm the full width at half maximum of each component, $\tau_1 = 5.0$ ns, and the emission maximum of component 1, $\lambda_1 = 470$ nm. Unless indicated otherwise, the simulated data contained 2% random noise, $\tau_2 = 10.0$ ns, and $\lambda_2 = 490$ nm. The simulated data covered 13 wavelengths between 450 and 510 nm at 5-nm increments, seven frequencies between 3.0 and 93.0 MHz at 15-MHz intervals and 12 θ_D per frequency (six I_p between 0 and 100° and six I_q between 90 and 190° at 20° increments). Simulations were also performed by varying τ_2, λ_2, or the percent noise. The simulated data were analyzed as the experimental data; however in some cases the number of frequencies, θ_D, or wavelengths used in the analysis were restricted.

As a measure of the resolvability of the data, we used the standard deviations (SD) of the calculated values. The SD were calculated from the diagonal elements of the covariance matrix (39) and do not include the effects of correlation between the parameters (42). The standard deviations of $f_2(\lambda)$ at 470, 480, and 490 nm were divided by the values of $f_2(\lambda)$ at these wave lengths and then averaged to give the fractional standard deviation (SD/$f_2(\lambda)$). From 470 to 490 nm the values of $f_2(\lambda)$ vary from 30 to 70%, so these wavelengths represent areas of strong spectral overlap. Similarly, (SD/τ_i) is the average of the standard deviations of the lifetimes divided by the calculated values of the lifetimes.

RESULTS

Resolution of Mixtures.

Phase sensitive detection of fluorescence has not been previously used to recover the unknown spectra and lifetimes of components in a mixture. Hence, the resolution and thus the usefulness of this technique were unknown, primarily because of the larger number of floating parameters needed to describe the unknown emission spectrum of each component. We examined a two-component mixture of FLS and 9-AA in ethanol to determine whether the lifetimes and “unknown” emission spectra could be determined. The data were collected from 480 and 560 nm (17 wavelengths) at 9 frequencies and 12 detector phase angles per frequency. The wavelength-dependent phase sensitive intensities, and the frequency-dependence of these values, contain information on the lifetimes and emission spectra of each component in the mixture. The data were analyzed with the lifetimes and all wavelength-dependent fractional intensities as floating parameters. For comparison we also measured the lifetimes and steady-state intensities of single component solutions of FLS and 9-AA at the same concentration as the probes were in the mixture. These independent measurements were used to determine the accuracy of the values calculated from the two-component fits of the VFPS data.

Figure 1 shows the emission spectra of FLS and 9-AA, as well as the spectrum of the mixture, $I_{ss}(\lambda)$. The wavelengths used in the analysis (480–560 nm) are only in regions of spectral overlap of the FLS and 9-AA emission spectra. This wavelength restriction

increases the difficulty of the resolution, as we purposefully eliminated data which contained information on only one component in the mixture. Such single-component data define the characteristics of the one component and greatly simplify the resolution. Analysis of the data with a single decay time model yielded $\chi_R^2 = 5.72$ (Table I). When the data were fit to a two-component decay, χ_R^2 decreased over 10-fold to 0.542. Importantly, the calculated lifetimes from the two-component fit, 4.51 and 9.30 ns, are close to the independently measured values of 4.54 and 9.85 ns, demonstrating that the lifetimes can be reliably recovered from the analysis. When the data were fit to a three-component decay, χ_R^2 decreases only 1.08-fold to 0.501. Statistically, a decrease in χ_R^2 of this amount is not highly significant with 1817 degrees of freedom (39). In addition, the fractional intensity of the first component was rather small (0.005 to 0.045) and the intensity constant across the spectrum. Also, the standard deviation of the decay times increased about 5-fold and in some cases the standard deviations of $f_2(\lambda)$ and $f_3(\lambda)$ increased to 50–130% of the corresponding values of the fractional intensities. This is in contrast to the two-component fit, where the standard deviations of $f_2(\lambda)$ were approximately 6% of the values. Hence, we conclude the data are best described by the two-component fit shown. This experiment was repeated and consistent results were obtained.

The wavelength-dependent fractional intensities from the two-component fit were used to calculate the emission spectra of each component, $I_i(\lambda)$ (Figure 1). The emission spectra and amplitudes associated with τ_1 (4.51 ns) and with τ_2 (9.30 ns) are in close agreement with the spectra of FLS and 9-AA, respectively. Hence, the fractional intensities were recovered with the precision adequate to determine the individual emission spectra and the relative yields.

As a second example, we examined a two-component mixture of TNS and PRODAN. Figure 2 shows the steady-state spectra of PRODAN and TNS (—) as well as of the mixture. The independently measured lifetimes of the two components are 3.45 and 7.89 ns, respectively. In this case the PS data were for 23 wavelengths, between 400 and 510 nm, eight frequencies, and 10 detector phase angles. Phase sensitive spectra of the mixture measured at two modulation frequencies, 18 and 33 MHz, are shown in Figure 3 to illustrate the appearance of the data. At each frequency the spectra were measured at 0, 80, 110, 130, and 180° relative to the phase angle of POPOP. The phase lag of POPOP at 18 MHz is 8.68° and 15.6° at 33 MHz. Therefore, the true detector phase angles are 8.7, 88.7, 119, 139, and 189° at 18 MHz and 15.6, 95.6, 126, 146, and 196° at 33 MHz. The dependence of the shape of the PS spectra on the value of ϕ_D is evident by examination of the spectra at 0, 80, 110, 130, and 180°. As the value of ϕ_D increases, the intensity of the shorter-lived PRODAN emission at the longer wavelengths decreases and becomes negative before the intensity of the TNS emission at the blue edge of the spectrum, with the longer lifetime. The phase angles are dependent on the modulation frequency. For example, the phase lag of both emissions is smaller at 18 than at 33 MHz. At 18 MHz and 119° (110° in Figure 3) the PS spectrum contains regions of both positive and negative intensity, while at 33 MHz and 126° (110° in Figure 3) the PS spectrum is positive and small at all wavelengths. The frequency-dependent demodulation between the 18 and 33 MHz signals is seen by comparing the phase sensitive spectra at 18 and 33 MHz at similar detector phase angles.

A one-component fit of these phase sensitive data yields $\chi_R^2 = 4.74$. When a second component is added χ_R^2 drops 4.8-fold to 0.986. The lifetimes from this fit, $\tau_1 = 3.83$ and $\tau_2 = 8.08$ ns, are close to the independently measured lifetimes of the single-component solutions, 3.45 ns for PRODAN and 7.89 ns for TNS (Table I). A three-component fit of the data, using 20 wavelengths, resulted in a 1.04-fold drop of χ_R^2 from a comparable two-component fit. In this case $I_1(\lambda)$ again becomes small and relatively constant across the spectrum. In addition, in the three-component fit, the recovered values of $I_2(\lambda)$ are larger than the intensities of the mixture. $I_{ss}(\lambda)$ values over the shorter wavelengths then become negative over the longer wavelength region of the spectrum. Conversely, the intensities of the third component, $I_3(\lambda)$ are negative at the blue edge and larger than $I_{ss}(\lambda)$ at the red edge of the spectrum. While the standard deviations in $f_2(\lambda)$ for the two-component fit are about 10% of the values of $f_2(\lambda)$, the standard deviations in $f_2(\lambda)$ and $f_3(\lambda)$ increase to over 100% of the corresponding values for the three-component fit. Because of the small decrease in χ_R^2 and the unreasonable parameters from the three-component analysis, we accept the two-component fit as the best description of the data.

Figure 2 shows the known emission spectra of TNS and PRODAN (—) as well as the recovered spectra (○, □). The 3.83-ns component is associated with the longer wavelength PRODAN emission, and the 8.08-ns component associates with the shorter wavelength TNS emission. These spectra closely match that of PRODAN and TNS, although the fit of the measured and calculated spectra appears worse at the shorter wavelengths.

The two-component mixtures described above are difficult cases because the decay times are different by only 2-fold and because of the high degree of spectral overlap. However, the measurements were facilitated by the stability and moderate intensity of the He–Cd laser light source. We are interested in resolving the still more complex emission from proteins, which is due primarily to tyrosine and tryptophan residues. Hence, we examined a two-component solution of NATyrA and NATA. This requires UV excitation, which was provided by a frequency-doubled dye laser. Additionally, we use the intrinsic harmonic content of the 3.79-MHz 5-ps pulse train (16), instead of the more common approach of intensity modulation of the incident light (15). Also, the decay times of 1.51 (NATyA) and 2.92 ns (NATA) are somewhat more closely spaced than for the mixtures in Figures 1 and 2.

Phase sensitive spectra were measured from 290 to 410 nm (25 wavelengths), at 12 detector phase angles and seven frequencies. When the data are fit to a two-component decay, χ_R^2 drops 8.9-fold from 23.4 to 2.62 (Table I). The lifetimes recovered from the two-component fit, 1.71 and 3.48 ns, are larger than the values expected from independent measurements of NATyrA and NATA (measured under the same conditions) of 1.51 and 2.92 ns, but the agreement is reasonable.

The calculated spectra (○, □) are in reasonable agreement with the expected spectra (—, Figure 4). The calculated and measured spectra match in the longer wavelength region of the emission. However, the calculated and measured spectra are not well matched for NATyrA near 300 nm. The Raman peak for 285-nm excitation in water should appear at about 318 nm and may be the origin of the deviations seen at 315 nm. It is clear that even for this relatively simple two-component mixture the match between the measured and calculated

data is not as close as might be desired. Although χ_R^2 drops a further 1.5-fold for a three-component fit (Table I) the recovered values from this fit are more unreasonable then those from the three-component fits already described. For example, the standard deviations of the lifetimes increased 10-fold over those in the two-component fit. More importantly, the recovered values of $I_2(\lambda)$ and $I_3(\lambda)$ become almost equal and opposite between 290 and 360 nm. This accompanies an increase in the intensities of the second component over the values of $I_{ss}(\lambda)$. In addition to the unrealistic values of $I_2(\lambda)$ and $I_3(\lambda)$, the standard deviations in the second- and third-component fractional intensities become greater than the actual values of $f_2(\lambda)$ and $f_2(\lambda)$ over most of the spectrum. ($f_2(\lambda)$ ranges from 2.0 to 0.89 with the SD of $f_2(\lambda)$ between 0.98 and 110; the values of $f_3(\lambda)$ are between −1.4 and 0.11 with the SD of $f_3(\lambda)$, 0.95 to 14). Based on these observations and other past experience, we do not accept fits in which χ_R^2 decreases less than 2-fold. We therefore reject the three-component results in favor of the two-component fit as the best description of these data.

We questioned whether the fit could be improved by holding one of the lifetimes constant at the independently measured value, which is presumably the correct value. The calculated spectra then showed still greater deviations from the measured spectra, and the values of χ_R^2 were higher. For example, for the NATyrA/NATA mixture, if τ_2 was held constant at 2.76 ns during the fit (the value from a VFPS fit for NATA alone), the value of τ_1 was 1.46 ns and χ_R^2 increased to 8.8. Alternatively, if τ_1 was held constant at 1.51 ns, only 0.2 ns from the value calculated in the original fit of the data, the calculated value of τ_2 was 3.45 ns and χ_R^2 increased slightly to 2.77. However, in both these fits the calculated values of $f_I(\lambda)$ were a worse match to the independently measured spectra. Thus, the results from the fits allowing both lifetimes to float were not due to local minima, but are the best fits of the data using our algorithm and the available data. In general, the recovered lifetimes appear to be more reliable than the recovered spectra. This is probably because the data at all wavelengths contribute to determining the decay times, whereas the amplitudes are determined at each wavelength by the phase sensitive data at that wavelength.

Analysis of Simulated VFPS Data.

The above results demonstrate that the variable-frequency phase-sensitive data can be used to recover decay times and unknown emission spectra. However, the resolutions were not as precise as desired and we were not able to consistently recover the unknown spectra and lifetimes from three-component mixtures (results not shown). To further understand the factors affecting the resolution, we analyzed simulated data. Several factors affect the resolution, such as the number of phase angles, modulation frequencies, and the range of emission wavelengths. The most important factors seem to be the difference between the decay times and the extent of noise in the data. It is difficult and probably not useful to present simulations in which all these parameters are varied. Instead, we simulated a set of VFPS data for a two-component mixture that is a slightly more difficult resolution problem than the experimental data presented above. We then reduced in turn the number of frequencies, wavelengths, and phase angles and moved the decay times closer to each other. These simulated data illustrate how the resolution is affected by the contributions from all these factors.

The first simulation of a two-component mixture used lifetimes that differed by a factor of 2, τ_1 = 5.0 ns and τ_2 = 10.0 ns. The simulated emission maxima were 20 nm apart (Δλ). The VFPS data were generated with 2% random noise, 12 detector phase angles, 7 frequencies, and 13 wavelengths. These simulated data were analyzed as the experimental data. The parameters were accurately recovered; τ_1 was 4.98 (±0.058) ns and τ_2, 10.3 (±0.19) ns. The calculated spectra of both components (○) overlap closely with the simulated spectra (Figure 5, —) and we consider these data to be resolvable.

To examine what factors limit the resolution, the parameters describing this data set were individually varied, followed by analysis of the modified data. We needed a definition of "resolvable". We arbitarily chose the ratio of the standard deviation of each parameter (calculated from the usual assumptions of nonlinear least squares) to the parameter value (SD/f_2(λ)). If this ratio exceeded 10%, the simulated data were said to be unresolvable.

The results of these analyses are summarized in Table II. For the complete set of simulated data SD/f_2(λ) is 0.099, or the standard deviations in f_2(λ) are about 10%. For lifetimes the ratio SD/τ_i is 0.015. This data set is said to be resolvable.

When the value of τ_2 was reduced to 9.0 or 8.5 ns (τ_2/τ_1 = 1.8 or 1.7), the relative uncertainty (SD/f_2(λ)) increased to 13 and 17%. Thus at τ_2/τ_1 = 1.8 the data become unresolvable. For τ_2 = 8.5 ns, the resolved values of τ_1 and τ_2 are 5.01 (±0.084) and 8.12 (±0.16) ns. The spectra calculated from the fit, I_i(λ), are shown in Figure 5 (□). As the lifetimes are brought closer together, the fractional intensities begin to deviate from the simulated values.

Similarly, we found the simulated mixture to be marginally (M) resolvable if the difference between the emission maxima (Δλ) is decreased to 10 nm and unresolvable for Δλ = 5 nm (Table II). If the number of frequencies is reduced to 4, the number of detector phase angles decreased to 6, or the percent noise in the data raised to 3%, the mixture becomes unresolvable. If the number of wavelengths is reduced to 11 or 9, the calculated lifetimes as well as fractional intensities do not match the expected values. This is due to the reduced range of the emission covered in the analysis. As the number of wavelengths is reduced, the regions where one component dominates the emission can be lost, making the resolution more difficult.

Evidently, resolution of even relatively simple two-component mixtures requires a substantial amount of data. For our experimental data (Figures 1–4) the percent noise was between 2 and 3%, the data consisted of spectra at 7–9 frequencies, 10–12 detector phase angles, and 17–23 wavelengths. In addition, τ_2/τ_1 ranged from 1.9 to 2.3 and Δλ from about 30 to 55 nm. Thus the mixtures should be resolvable, particularly due to the larger range of wavelengths. In fact, we found that the values of SD/f_2(λ) for the experimental data were 0.057 for the FLS/9-AA mixture and 0.11 for the other two solutions. The deviations between the expected and calculated parameters for the PRODAN/TNS and NATyrA/NATA mixtures thus may be partially explained by the data being close to the limit of resolvability.

One other explanation for the lack of precision in the recovered values could be due to correlation among the parameters, such that the value of one parameter can vary to

accommodate a change in another one, without affecting the value of χ_R^2. We therefore examined the correlation coefficients for the fits of three sets of experimental data. Substantial correlation between the parameters yields values of 0.9–1.0. Between τ_1 and τ_2 the values were 0.603, 0.398, and 0.490 for the FLS/9-AA, PRODAN/TNS, and NATyrA/NATA mixtures, respectively. The correlation coefficients between $f_2(\lambda)$ and the lifetimes ranged from −0.84 to −0.50, −0.67 to −0.16, and −0.91 to −0.54 for these mixtures. The values are relatively low, indicating the parameters are not highly correlated according to this criteria.

CONCLUSIONS

Multifrequency phase sensitive fluorescence can be used to resolve two-component mixtures when the lifetimes, fractional intensities, and spectral distributions are unknown. This method was developed as a possible alternative, and perhaps more rapid technique, than measurements of phase and modulation values at multiple frequencies and wave lengths for multicomponent analysis (12, 15). A large number of phase sensitive spectra are needed to determine the many parameters associated with the unknown emission spectra. Hence, even for two-component mixtures about 8 h were needed to collect adequate data. This is about 2-fold less than that needed to measure frequency-dependent phase and modulation data at a similar number of wavelengths. We have not attempted to optimize the acquisition rates for either type of experiment, and data acquisition is only partially automated.

At present, we are disappointed by the lack of precision in the recovered spectra and lifetimes, and for this reason we did not extend the technique to three-component mixtures. It is possible that we have not used the optimal arrangement for measuring the phase sensitive intensities. The phase angle control on our lock-in amplifier is rather coarse, and this device was not designed for accurate phase angle determinations. Improved phase angle precision, coupled with circuits to unambigiously eliminate instrumental drift during the lengthy data collection, may yield substantial improvements in resolution. Similarly, it may be advantageous to retain the absolute intensities of the phase sensitive spectra. In the present analysis, we cancelled the effects of frequency-dependent demodulation by dividing by the magnitude spectra. Retention of the intensity information is likely to further constrain the fits and hence improve resolution.

The resolution might also be improved by alternative methods of data analysis. We relied solely on nonlinear least squares. However, the multidimensional nature of the data makes it suitable for matrix methods such as factor analysis and related methods (43, 44). If the resolution of this method can be improved, then it seems probable that it would be generally useful for multicomponent analysis of mixtures and in the study of photosynthetic systems (37).

Acknowledgments

This work was supported by the National Science Foundation, Biophysics and Biological Instrumentation Programs (PCM 82-10878, DBM-8502835, and DBM-8511065), and a grant from the National Institutes of Health (GM-29318). Henryk Cherek expresses appreciation for financial support from Research Project CPBP 01.06.2.03 (Poland).

APPENDIX

In the analysis we use the PS ratio spectra, R_p and R_q, which are compared with the calculated values, R_{cp} and R_{cq}. Recalling that for a single exponential decay $m_i = \cos\ \theta_i$ and $\tan\ \theta_i = \omega\tau_i$, the ratio spectrum R_{cp} is given by

$$R_{cp}(\lambda, \theta_D, \omega) = \frac{\sum_i f_{ci}(\lambda) \cos\ (atn(\omega\tau_{ci}))\ \cos\ (\theta_D - atn(\omega\tau_{ci}))}{\sum_i f_{ci}(\lambda) \cos\ (atn(\omega\tau_{ci}))} \quad \text{(A1)}$$

The expression for the quadrature spectrum is similar except θ_D is replaced with $\theta_D + 90°$. The equation is presented in terms of $f_i(\lambda)$ and τ_i because we need the derivatives with respect to these parameters, and our program is written in terms of these parameters.

The nonlinear least-squares routine, written in Basic-11, runs on a DEC 11/73 computer and may be obtained from J.R.L. The program uses analytical derivatives with respect to τ_{ci} and $f_{ci}(\lambda)$. The derivatives are given by

$$\partial R_{cp}/\partial\tau_{ci} = \frac{A - BR_{cp}}{\sum_i f_{ci}(\lambda) \cos\ (atn(\omega\tau_{ci}))} \quad \text{(A2)}$$

where

$$A = \frac{f_{ci}(\lambda)\omega \sin\ (\theta_D - 2atn(\omega\tau_{ci}))}{(1 + \omega^2\tau_{ci}^2)} \quad \text{(A3)}$$

$$B = -\frac{f_{ci}(\lambda)\omega \sin\ (atn(\omega\tau_{ci}))}{(1 + \omega^2\tau_{ci}^2)} \quad \text{(A4)}$$

and

$$\partial R_{cp}/\partial f_{ci}(\lambda) = \frac{C - DR_{cp}}{\sum_i f_{ci}(\lambda) \cos\ (atn(\omega\tau_{ci}))} \quad \text{(A5)}$$

where

$$C = \cos(atn(\omega\tau_{ci}))\cos\ (\theta_D - atn(\omega\tau_{ci})) \quad \text{(A6)}$$

and

$$D = \cos\ (atn(\omega\tau_{ci})) \quad \text{(A7)}$$

For nonlinear least-squares analysis the usual weighting factor is $1/\sigma^2$, where $(\sigma^2)^{1/2}$ is the standard deviation of the measurement (39). The selection of a weighting factor for analysis of the single frequency PS data has been discussed in detail (36). In the previous analysis the

I_p and I_q spectra were analyzed, rather than the ratio spectra. Then, the weighting factor σ was

$$\sigma = 0.01S\left(\overline{I_m(\lambda)}\right)^{1/2} \quad \text{(A8)}$$

where $\overline{I_m(\lambda)}$ is the average of $I_m(\lambda)$ over the measured wavelengths. In the present analysis, the ratio spectra are fit, and therefore I_m is dropped from the weighting factor as described by eq 10. The values of χ_R^2 were mostly constant at all frequencies. Hence, we believe that the level of noise in the ratio spectra is independent of frequency, and we used a frequency-independent weighting factor.

Although the chosen value of the percent (S) will affect the magnitude of χ_R^2, the value of S does not affect the relative values of χ_R^2 for one-, two-, or three-component fits of the same data. Thus, the value of S does not limit the selection of the correct number of components in the sample. We choose the value of S from experience. For example, if a two-component fit of a known two-component sample yields a χ_R^2 near 1.0 with 2% noise, then we can assume the noise level is actually near 2%. We consistently found noise levels between 1 and 3% for the VFPS data.

LITERATURE CITED

(1). Lakowicz JR Principles of Fluorescence Spectroscopy; Plenum Press: New York, 1983.

(2). Steiner RF, Kubota Y In Excited States of Biopolymers; Steiner RF, Ed.; Plenum Press: New York, 1983; pp 203–254.

(3). Lin T; Dowben RM In Excited States of Biopolymers; Steiner RF, Ed.; Plenum Press: New York, 1983; pp 59–115.

(4). O'Connor DV; Phillips D Time-Correlated Single Photon Counting; Academic Press: New York, 1984.

(5). Brand L; Knutson JR; Davenport L; Beechem JM; Dale RE; Walbridge DG; Kowalczyk AA In Spectroscopy and the Dynamics of Molecular Biological Systems; Bayley, Dale RE, Eds.; Academic: New York, 1985; pp 259–303.

(6). Knutson JR; Beechem JM; Brand L Chem. Phys. Lett 1983, 102, 501–507.

(7). Demas JN Excited State Lifetime Measurements; Academic: New York, 1983.

(8). Weber GJ Phys. Chem 1981, 85, 949–953.

(9). Jameson DM; Gratton E In New Directions in Molecular Luminescence; Eastwood P, Ed.; American Society for Testing and Materials: Philadelphia, PA, 1983; pp 67–81.

(10). Beechem JM; Knutson JR; Ross JBA; Turner BW; Brand L Biochemistry 1983, 22, 6054–6058.

(11). Dalbey RE; Weiel J; Perkins W; Yount RG J. Biochem. Biophys. Methods 1984, 9, 251–266. [PubMed: 6547966]

(12). Lakowicz JR; Laczko G; Cherek H; Gratton E; Limkeman M Biophys. J 1984, 46, 463–477. [PubMed: 6498264]

(13). Gratton E; Limkeman E; Lakowicz JR; Maliwal B; Cherek H; Laczko G Biophys. J 1984, 46, 479–486. [PubMed: 6498265]

(14). Gratton E; Limkeman M Biophys. J 1983, 44, 315–324. [PubMed: 6661490]

(15). Lakowicz JR; Maliwal BP Biophys. Chem 1985, 21, 61–78. [PubMed: 3971026]

(16). Lakowicz JR; Laczko G; Gryczynski I Rev. Sci. Instrum 1986, 57, 2499–2506.

(17). Lakowicz JR; Laczko G; Gryczynski I Biophys. Chem 1986, 24, 97–100. [PubMed: 3756310]

(18). Libertini LJ; Small EW Biophys. J 1985, 47, 765–772. [PubMed: 4016197]

(19). Ludescher RD; Volwerk JJ; de Haas GH; Hudson BS Biochemistry 1985, 24, 7240–7249. [PubMed: 4084578]
(20). Albana J; Albert B; Krajcarski DT; Szabo AG FEBS Lett. 1985, 182, 302–304. [PubMed: 3979553]
(21). Jameson DM; Weber GJ Phys. Chem 1981, 85, 953–958.
(22). Eftink MR; Jameson DM Biochemistry 1982, 21, 4443–4449. [PubMed: 6751389]
(23). Veselova TV; Cherkasov AS; Shirokov VI Opt. Spectrosc 1970, 29, 617–618.
(24). Lakowicz JR; Cherek HJ Biochem. Biophys. Methods 1981, 5, 19–35.
(25). Lakowicz JR; Cherek HJ Biol. Chem 1981, 256, 6348–6353.
(26). Lakowicz JR; Keating SJ Biol. Chem 1983, 258, 5519–5524.
(27). McGown LB; Bright FV Anal. Chem 1984, 56, 2195–2199.
(28). McGown LB; Bright FV Anal. Chem 1984, 56, 1400A–1415A.
(29). Bright FV; McGown LB Anal. Chem 1985, 57, 2877–2880.
(30). Gratton E; Jameson DM Anal. Chem 1985, 57, 1694–1697.
(31). Demas JN; Keller RA Anal. Chem 1985, 57, 538–545.
(32). Van Hoek A; Visser AJWG Anal. Instrum. (N.Y.) 1985, 14, 143–154.
(33). Lakowicz JR; Thompson RB; Cherek H Biochim. Biophys. Acta 1983, 734, 295–308.
(34). Lakowicz JR; Balter A Chem. Phys. Lett 1982, 92, 117–121.
(35). Keating-Nakamoto S; Cherek H; Lakowicz JR Anal. Biochem 1985, 148, 349–356. [PubMed: 4061815]
(36). Keating-Nakamoto SM; Cherek H; Lakowicz JR Biophys. Chem 1988, 24, 79–95.
(37). Moya I In Time-Resolved Fluorescence Spectroscopy in Biochemistry and Biology; Cundall RB, Dale RE, Eds.; Plenum: New York, 1980; pp 755–768.
(38). Spencer RD; Weber G Ann. N.Y. Acad. Sci 1969, 158, 361–376.
(39). Bevington PR Data Reduction and Error Analysis for the Physical Sciences; McGraw-Hill: New York, 1969; Chapter 11, pp 204–246.
(40). Spencer RD, Weber GJ Chem. Phys 1970, 52, 1654–1663.
(41). Lakowicz JR; Cherek H; Balter AJ Biochem. Biophys. Methods 1981, 5, 131–146.
(42). Johnson ML Biophys. J 1983, 44, 101–106. [PubMed: 6626675]
(43). Malinowski FR; Howery DG Factor Analysis; Wiley: New York, 1980.
(44). Marchiarullo MA; Ross RT Biochim. Biophys. Acta 1985, 807, 52–63.

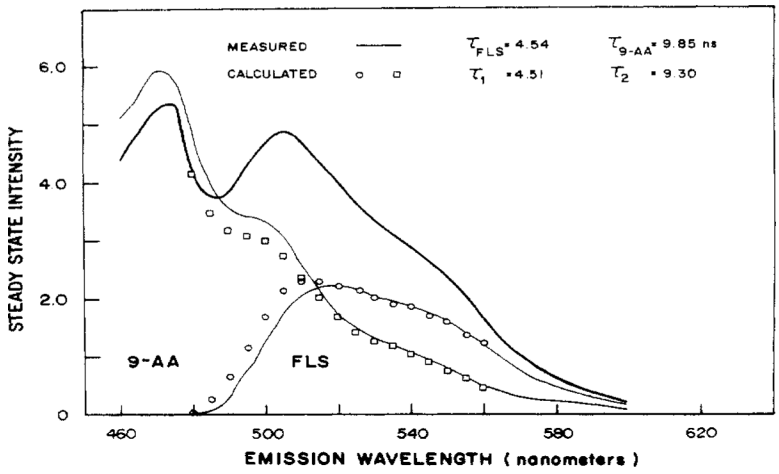

Figure 1.

Determination of the lifetimes and emission spectra of a two-component mixture. The separately measured spectra of FLS (—), 9-AA (—), and the mixture (—) are shown. The calculated spectra are also shown for the 4.51 ns (○) and 9.30 ns (□) components. All solutions were in 100% ethanol. The lifetimes and emission spectra were variables In the analysis.

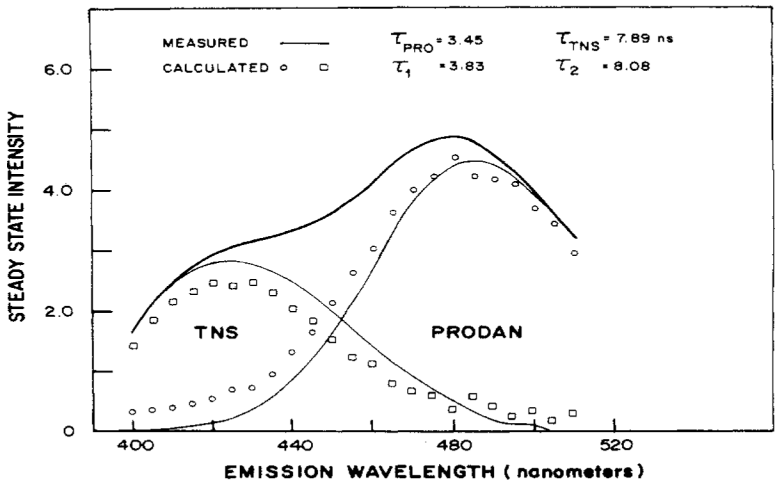

Figure 2.

Resolution of TNS and PRODAN mixture. The separately measured emission spectrum of the mixture is shown as a bold line (—), and the spectra of TNS and PRODAN as thinner lines (—). The calculated spectra are shown for the 8.08 ns (□) and 3.83 ns (○) components. The solutions were In 100% ethanol.

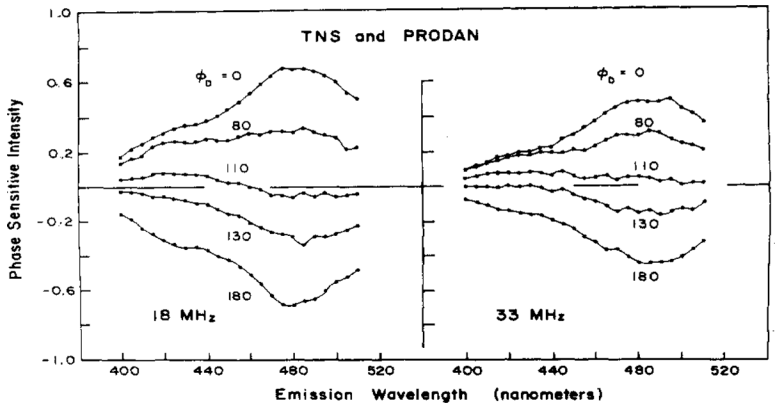

Figure 3.

Phase sensitive spectra of TNS and PRODAN mixture. Phase sensitive spectra of the TNS and PRODAN mixture measured at 18 MHz (left) and 33 MHz (right). The spectra were measured at 0, 80, 110, 130, and 180° relative to POPOP. The true phase angles relative to the Incident light are 8.7, 88.7, 119, 139, and 189° at 18 MHz and 15.6, 95.6, 126, 146, and 196° at 33 MHz.

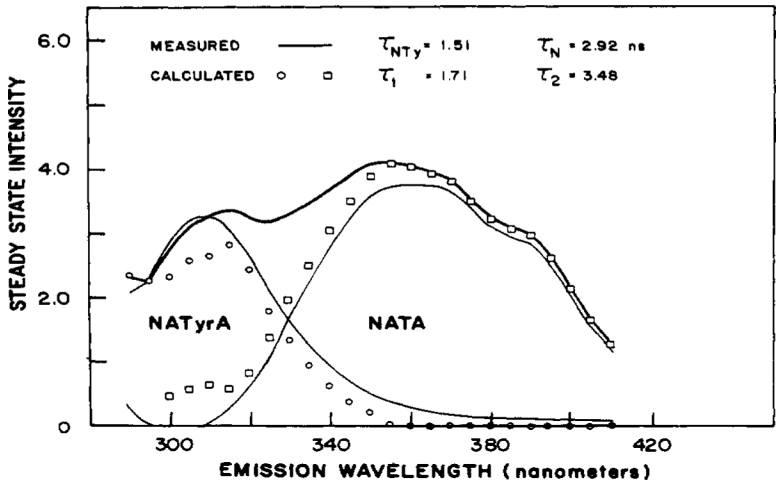

Figure 4.

Resolution of a mixture of NATyrA and NATA: steady-state spectra of the mixture (—) and NATyrA and NATA (—). Calculated spectra were as follows: 1.71 ns (○); 3.48 ns (□). The buffer was 25 mM Tris-HCI, pH 7.5.

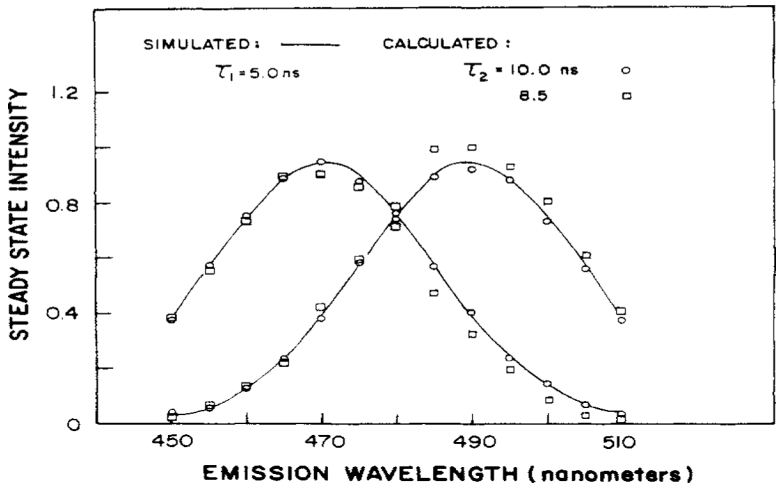

Figure 5.

Analysis of simulated phase sensitive spectra: simulated emission spectra (—). Calculated emission spectra were as follows: τ_1 = 5 ns and τ_2 = 10 ns (○), τ_1 = 5 ns and τ_2 = 8.5 ns (□).

Table I.

Resolution of Two-Component Mixtures by VFPSD

compounds	component fit	measd τ_i ns	calcd τ_i ns	χ_R^2
FLS/9-AA[a]	1		6.05	5.72
	2	4.54[b] (0.02)	4.51 (0.032)[c]	0.54
		9.85 (0.02)	9.30 (0.092)	
	3		2.03 (0.44)	0.50
			5.23 (0.20)	
			9.76 (0.22)	
PRODAN/TNS[d]	1		4.88	4.74
	2	3.45 (0.068)	3.83 (0.041)	0.99
		7.89 (0.11)	8.08 (0.16)	
	3		2.55 (0.66)	0.94
			6.69 (0.53)	
			4.19 (0.31)	
NATyrA/NATA[d]	1		2.74	23.4
	2	1.51 (0.19)	1.71 (0.024)	2.6
		2.92 (0.18)	3.48 (0.013)	
	3		1.34 (0.045)	1.7
			3.40 (0.16)	
			4.21 (0.34)	

[a]The VFPS data were analyzed from 480 to 560 nm (17 wavelengths) with an assumed noise level of 2%. 54 files were used in the analysis, representing six θ_D between 0 and 100° for I_p and six θ_D between 90 and 190° for I_q, at nine F from 2.0 to 92.0 MHz.

[b]Lifetimes of single-component solutions measured under the same conditions as the VFPS data.

[c]The values in parentheses are the standard deviations calculated from the diagonal terms of the covarience matrix (39).

[d]As in footnote a, but 40 files were used in the analysis with data from 10 θ_D (for I_p between 0 and 80°) at 8 F between 3.0 and 108.0 MHz and 23 wavelengths between 400 and 510 nm, assuming 3% noise.

[e]As in footnote *a* but 48 files were used including data from 7 F between 11.37 and 113.7 MHz, over 25 wavelengths between 290 and 410 nm, assuming 2% noise.

Table II.

Analysis and Resolvability of Simulated Data

τ_2/τ_1	$\Delta\lambda$	F	θ_D	% noise	λ	SD/τ_i	SD/$f_2(\lambda)$	Res[a]
2.0[b]	20	7	12	2	13	0.015	0.099	+
1.8[c]						0.016	0.13	M
1.7						0.018	0.17	−
2.0[d]	10					0.021	0.12	M
	5					0.031	0.18	−
2.0[e]	20	5				0.016	0.10	M
		4				0.016	0.16	−
2.0[f]	20	7	8			0.018	0.13	M
			6			0.021	0.13	−
2.0	20	7	12	3		0.022	0.14	M
				4		0.030	0.21	−
2.0[g]	20	7	12	2	11	0.018	0.12	M/−
					9	0.026	0.18	−

[a] If Res is +, M, or −, the data are resolvable, marginally resolvable, or not resolvable

[b] For all simulated data, τ_1 = 5.0 and τ_2 = 10 ns and λ_1 = 470 and λ_2 = 490 nm. Data for seven F between 3.0 and 93.0 MHz, 12 θ_D total (six θ_D between 0 and 100° for I_p data), and 13 wavelengths between 450 and 510 nm, were fit except as indicated. See text for further details.

[c] Data as in footnote *b* but τ_2 = 9.0 (τ_2/τ_1 = 1.8) or 8.5 (τ_2/τ_1 = 1.7) ns.

[d] As in footnote *b* but λ_2 = 480 ($\Delta\lambda$ = 10) or 475 ($\Delta\lambda$ = 5) nm.

[e] Data fit as in footnote *b* but using five (3, 18, 33, 63, 93 MHz) or four (3, 33, 63, 93 MHz) frequencies (F).

[f] Data fit using eight (for L at 0, 20, 60, 100°) or six (for I_p at 20, 60, 100°) detector phase angles (θ_D).

[g] The number of wavelengths were 11 (from 455 to 505 nm) or 9 (from 460 to 500 nm).